Desalination and Water Treatment
www.deswater.com

doi: 10.5004/dwt.2019.24718

170 (2019) 91–100
December

Effect of salinity and temperature on air dissolution in an unpacked air saturator of a dissolved air flotation system

Vahid Reza Fanaie, Mehdi Khiadani*, Guangzhi Sun

School of Engineering, Edith Cowan University, Joondalup, Perth, WA, Australia, emails: m.khiadani@ecu.edu.au (M. Khiadani), v.fanaieesfahani@ecu.edu.au (V.R. Fanaie), g.sun@ecu.edu.au (G. Sun)

Received 4 December 2018; Accepted 26 July 2018

ABSTRACT

The amount of the precipitated air inside a flotation tank has a significant effect on the removal efficiency of a dissolved air flotation (DAF) system. For the first time, this study examined the effect of salinity (35 g L^{-1}) and temperature variations (10°C–40°C) on air solubility in an unpacked air saturator of a real-scale DAF system for different range of pressures (300–600 kPa) and recycle ratios (10%–40%). The amount of dissolved air inside the air saturator was measured using the liquid displacement method. The results indicated that, under equilibrium conditions, salinity and temperature are inversely proportional to air solubility. However, under non-equilibrium status, with increases in temperature, the amount of dissolved air declines to its minimum value at 20°C and then increased again. The observed behaviour was attributed to the effect of temperature on volumetric gas/liquid mass transfer (K_La). The effects of recycle ratio and pressure was also investigated for non-equilibrium conditions and it was observed that the temperatures was below 20°C, an increase in recycle ratio and saturator pressure can compensate the lack of air caused by salinity and increase of temperature. However, for temperatures above 20°C, it is not necessary to increase the recycle ratio and saturator pressure as the rise of temperature by itself increases air concentration. Finally, the size distribution of microbubbles was also investigated and it was found that temperature does not affect the average size of microbubbles noticeably whereas salinity prevents coalescence and contributes to smaller size bubbles.

Keywords: Dissolved air flotation; Microbubbles; Salinity; Temperature; Air saturator

1. Introduction

Due to slow settling velocity of colloidal suspensions and emulsified oils, the removal of such particles by conventional sedimentation techniques are demand larger size tanks to provide more retention time, or consumption of more chemicals to increase the size of aggregates. To overcome this issue, one solution is to employ dissolved air flotation (DAF) systems, which is specifically designed for the removal of small size and light density particles [1].

In DAF systems, an air-saturator is used to dissolve air in water by applying high pressure (300–700 kPa). Thereafter, the mixture of air and water are released into a flotation tank which is exposed to atmospheric pressure. Due to the depressurization, the dissolved air starts to precipitate and form micro-bubbles. These formed micro-bubbles then attach to suspended particles and bring them to the surface (supernatant layer) due to buoyancy force. Finally, the formed layer of sludge on the surface is removed from the top by a scraper [2].

Over the past decade, the application of DAF has gone beyond normal drinking water treatment, and recently, it has been used as a pre-treatment unit for the removal of suspended particles in saline effluents and industrial discharges [3–5]. Salinity and temperature variations of seawater are two important parameters which can affect different aspects of the DAF process such as bubble size distribution (BSD),

* Corresponding author.

1944-3994/1944-3986 © 2019 Desalination Publications. All rights reserved.

bubble rising velocity and air dissolution. Among these, the effects of salinity and temperature on air dissolution are of great importance [6,7].

Dissolution of air in the air saturator, as the first step in the DAF process, is fundamental to DAF on two different counts. Firstly, it determines the volume of precipitated air inside the flotation tank. That is, the more precipitated air in the form of micro-bubbles provides more collision opportunities and therefore more attachment of micro-bubbles to particles [8]. Secondly, around 50% of operating costs can be attributed to air saturators [9]. The size distribution of micro-bubbles is also of great importance as it can directly affect collision opportunities and rising velocity [10,11]. Therefore, consideration of salinity and temperature of seawater in the design and operation of air saturators of the DAF system is highly important. Generally, air saturators are classified as packed and unpacked, where the key difference between these two is that packed saturators are filled with packing materials whereas unpacked saturators are left unfilled [12].

Existing literature on air dissolution in air saturators is limited, and the main focus of these studies has been mainly on developing mathematical models for the prediction of gas composition in saturators and air concentration. For example, Haarhoff and Steinbach [13] proposed a model based on molar gas mass balance across the air saturator in order to calculate the air concentration in packed saturators. In another recent study, Bahadori et al. [14] have used the Vandermonde matrix and proposed a polynomial function to estimate mass concentration of air in recycled flow by considering pressure and temperature as the independent variables.

Besides modelling air saturators, some previous studies have measured air concentration using different methods. Generally, there are two approaches for measuring air concentration. In the first approach, available air is directly measured once the saturator is under pressure (direct method), but this is a difficult technique practically and it was rarely followed. The second approach measures precipitated air after depressurization using the liquid displacement technique (indirect method). This can be implemented either continuously or in batch mode. For laboratory studies and small-scale DAF systems, the liquid displacement method is preferable [12]. Conway and Nelson [15] have applied this technique by directing the trapped air in the headspace of a flotation cylinder to an inverted burette. The volume of precipitated air was equal to the change in the volume of trapped air in the burette. A similar approach was followed by Lovett et al. [16] and Henry and Gehr [17]. Steinbach and Haarhoff [18] then modified the previous designs and improved the accuracy of measuring procedures.

Very few studies have investigated the effect of temperature on air saturators. For example, Shannon and Buisson [19] have studied the adaptation of DAF systems for the treatment of effluents from geothermal power stations. They investigated air dissolution in a packed saturator for temperatures of 50°C and 80°C. They observed that for the range of pressures below 350 kPa, the amount of dissolved air at 80°C was higher than 50°C, and this was attributed to the increased water vapour pressure. Dassey and Theegala [8] have studied the effect of temperature on air dissolution in an unpacked saturator. The range of the temperature in their experiments varied between 5°C and 35°C, for a constant pressure of 500 kPa. In their experiments, air concentration reached its minimum value at 21°C and increased again with an increase of temperature. None of the abovementioned has studies considered the effect of salinity on air concentration.

Haarhoff and Edzwald [6] theoretically studied the adaptation of DAF for seawater pre-treatment in desalination plants. The authors reported that the effect of salinity and temperature of seawater on air dissolution in air saturators cannot be overlooked in the design and operation of DAF systems. They assumed the air saturators are operated under equilibrium conditions and have applied Henry's laws of gas dissolution in the liquid phase to investigate the effect of salinity and temperature variations of seawater on air solubility. Moreover, they recommended the increase of saturator pressure and recycle ratio as two feasible approaches to compensate for the lack of available air caused by salinity and temperature. Nonetheless, it should be pointed out that, in practice, the operation of DAF systems under equilibrium condition may rarely occur as it demands long hydraulic retention time (HRT).

With regards to existing literature, only a limited number of studies have considered the effects of temperature on air dissolution in air saturators. Moreover, not only do many uncertainties still exist about the effects of temperature on air dissolution, none of these previous studies has investigated the effect of salinity on air dissolution within a DAF system. Therefore, the specific objective of this study is to investigate the effects of salinity and temperature on air dissolution in an unpacked air saturator by considering saturator pressure and recycle ratios. Finally, under the influence of temperature and salinity, the size distribution of microbubbles was obtained using the shadow imaging technique.

2. Material and methods

2.1. Theoretical background

Haarhoff and Steinbach [20] assumed equilibrium condition in the air saturators and developed the following equations based on Henry's law of gas dissolution in the liquid phase.

$$S = \frac{P_{\text{atm}} + P_{\text{sat}} - P_{\text{vap}}}{P_{\text{atm}}} \tag{1}$$

$$f_{\text{sat},N} = \frac{f_{\text{atm},N}[H_N(S - f_{\text{atm},ar} - f_{\text{atm},O}) + f_{\text{atm,Ar}} \times H_{\text{Ar}} + f_{\text{atm},O} \times H_O]}{S(f_{\text{atm},O} \times H_O + f_{\text{atm},N} \times H_N + f_{\text{atm,Ar}} \times H_{\text{Ar}})} \tag{2}$$

$$f_{\text{sat},O} = \frac{f_{\text{atm},O}}{S} + \left(\frac{H_O}{H_N}\right)\left(\frac{f_{\text{sat},N} \times f_{\text{atm},O}}{f_{\text{atm},N}}\right) - \left(\frac{H_O}{H_N}\right)\frac{f_{\text{atm},O}}{S} \tag{3}$$

$$f_{\text{sat,Ar}} = 1 - f_{\text{sat},N} - f_{\text{sat},O} \tag{4}$$

$$C_r^* = \left(P_{\text{sat}} - P_{\text{vap}}\right)\left(\frac{44.6}{101.3}\right)\left(\frac{273.2}{273.2 + T}\right)\left(\frac{f_{\text{sat},N}}{H_N} + \frac{f_{\text{sat},O}}{H_O} + \frac{f_{\text{sat,Ar}}}{H_{\text{Ar}}}\right) \tag{5}$$

where C_r^* is the theoretical mass concentration of the air (mol m^{-3}), P_{atm} is the atmospheric pressure (kPa), P_{sat} is the saturator pressure (kPa), P_{vap} is the vapour pressure of water (kPa), H_{Ar}, H_N and H_O are Henry's constants for argon, nitrogen and oxygen, respectively, $f_{atm,O}$, $f_{atm,N}$, and $f_{atm,Ar}$ are fraction of oxygen, nitrogen and argon gas in atmospheric air, and $f_{sat,O}$, $f_{sat,N}$, and $f_{sat,Ar}$ are the fraction of oxygen, nitrogen and argon gas in the air saturator, respectively. The Henry's constants for different temperatures and salinities are empirical values which can be obtained in multiple references [12,21]. The vapour pressure of water for different degree of salinities and temperatures can also be found in Nayar et al. [22].

2.2. Experimental setup

Fig. 1 shows the schematic representation of the experimental setup which comprises of a storage tank, a flotation tank, a saturator, an air compressor and an air quantification unit. An electrical heater (3 kW, Vulcanic TEE, Australia) was installed inside the water storage tank to achieve the desired water temperature. Ice cubes were then added to the storage tank to lower the water temperature. Sodium chloride (99% purity) was mixed with water in the storage tank to obtain the required salinity (35 g L^{-1}). A pump was installed inside the water storage tank to deliver water to the flotation tank which is made up of acrylic materials. Two centrifugal pumps recycled water from the flotation tank through a *T*-piece where the compressed air and recycled water were mixed before entering the air saturator. The amount of recycle ratio is defined as:

$$r(\%) = \frac{Q_r}{Q_{in}} \tag{6}$$

where Q_r (L h^{-1}) is recycled water flow rate and Q_{in} (L h^{-1}) is the influent flow rate.

The air saturator was a cylindrical column of 50 cm height and 16 cm diameter made of acrylic materials. A bleed valve was mounted on top of the air saturator to release the excess air to maintain constant pressure and also to control the formation of large size bubbles through the release of excess air. A plug valve was also installed at the top of the saturator to ensure it is completely filled with water. The air saturator was insulated with earth wool materials to maintain the desired temperature during the experiments. The saturator pressure was adjusted via a globe valve (V6) and the recycle flow was measured by a rotameter type flow meter (F2). A pressure gauge and a flow meter were used to measure and adjust the air flow into the saturator. Micro-bubbles were formed inside the flotation tank by lowering the saturator pressure to atmospheric pressure through a pressure relief valve.

The air quantification unit shown in Fig. 1 was designed and made of acrylic materials. A ball valve (V2) was installed on the top end of the graduated cylinder. A baffle split the lower section of the cylinder into two parts to prevent short-circuit of micro-bubbles and also helped to direct the micro-bubbles to the graduated measuring cylinder. A nozzle was fitted to the inlet of air quantification unit and a small plastic plate was positioned in front of the nozzle's orifice to enhance the precipitation. The design of this nozzle was similar to the one used by Haarhoff and Steinbach [13]. For

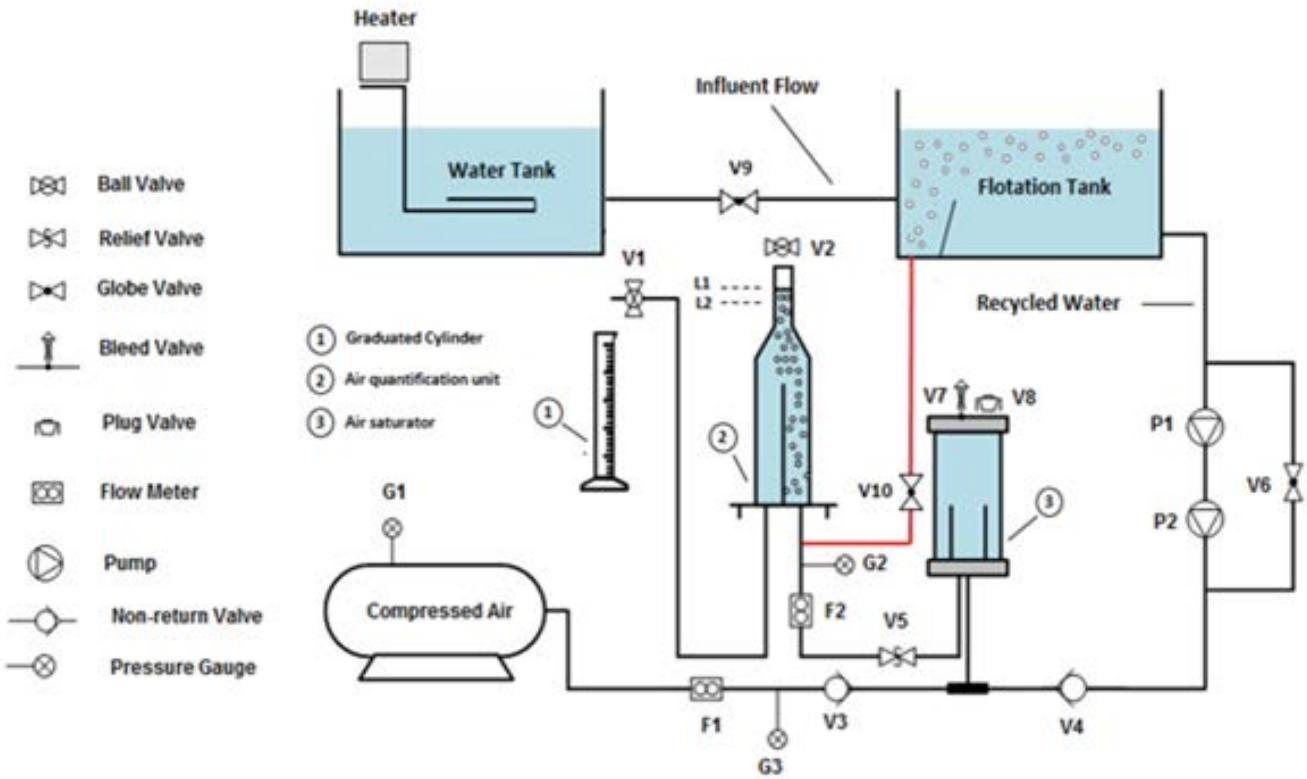

Fig. 1. Schematic of dissolved air flotation setup, air saturator and air quantification unit.

measuring available air, valve V10 was put in a closed position and the flow was directed to the air quantification unit. Initially both valves V1 and V2 were kept open and two arbitrary levels were determined on the graduating vertical cylinder by adjusting the overflow valve. The actual measurement was started when the water level adjusted to L1 and the valve V2 was in a closed position. The overflow water was collected in a graduated container until the water level slumped to L2 by adjusting the position of the measuring beaker. The difference between L1 and L2 correlates to the precipitated air volume, and the actual amount of air can be estimated from Eq. (7):

$$C_r = \left(\frac{V_{air}}{V_{water}}\right)\left(\frac{44.6}{0.95}\right)\left(\frac{273.2}{273.2+T}\right)\left(\frac{P_{atm}}{101.3}\right) \quad (7)$$

where C_r (mol m^{-3}) is the mass concentration of air in recycled flow, V_{air} is the air volume which is the difference between L1 and L2, V_{water} is the volume of collected water, T (°C) is the temperature, P_{atm} (kPa) is the atmospheric pressure. Coefficients 44.6 and 0.95 are the molar mass of the air and precipitation efficiency of the nozzle, respectively. The precipitation efficiency was obtained by a system of equations and a series of experiments through different operative conditions. Further information about measuring precipitation efficiency can be found in the study by Haarhoff and Steinbach [13]. Table 1 indicates the range of the parameters in this study with their intervals and uncertainties. All the measurements were repeated for three times.

2.3. Equilibrium and non-equilibrium experiments

In order to ensure equilibrium status, the air saturator was continuously aerated while both valves V4 and V5 were closed. The saturator pressure was set at 500 kPa by adjusting the bleed valve V7. After the allotted time, the air flow meter F1 was turned off and the valve V5 was opened to navigate the flow to the air quantification unit for measuring air concentration. The experiments were performed for temperatures ranging from 10°C–40°C in 10°C interval.

Attaining equilibrium conditions requires long HRT which is rarely achieved for most of the air saturators. Therefore, it is likely that most of the air saturators are operated in non-equilibrium conditions. To investigate the effects of salinity and temperature on air dissolution in non-equilibrium conditions, the air saturator was operated in normal conditions and the amount of precipitated air was quantified while valves V3, V4 and V5 remained open. In these experiments, the effects of pressure and recycle ratios were also considered.

2.4. Microbubbles size measurements

In order to measure the size distributions of microbubbles, as shown in Fig. 2, a high-speed camera (Speed sense 1,040, Sensor resolution: 2,320 × 1,726 pixels) was coupled with a long distance microscope (Questar QM-1, U.S.A.) to

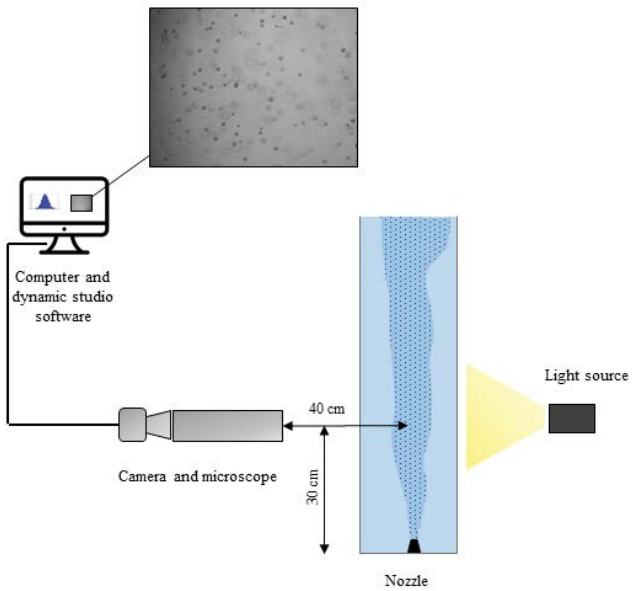

Fig. 2. Photography setup for capturing images (side view of flotation tank).

Table 1
Experimental parameters with their ranges, intervals and uncertainties

Parameters	Operating range	Intervals	Uncertainty (W_R)
Temperature, °C	10–40	10	±2.3%
Salinity, g L^{-1}	0 and 35	–	±1%
Pressure, kPa	300–600	100	±3%
Influent flow (f_{in}), L h^{-1}	400	–	±2%
Recycle flow (f_{Re}), L h^{-1}	40–160	40	±2.8%
Air flow, N L h^{-1}	100	–	±2.6%
V_{air}, mL	–	–	±3%
V_{water}, mL	–	–	±3.5%
C_r, mol m^{-3}	–	–	±3.8%

Measured values from the air quantification unit were converted from mol m^{-3} to mg L^{-1} by considering molar mass of the air (≈29 g mol^{-1})

capture photos from microbubbles. The camera was positioned and focused at 40 cm distance from the centre of the flotation tank (centre of the middle nozzle) and 30 cm above the bottom of the flotation tank. A light-emitting diode light source (Veritas, 5,600 k, U.S.A.) was located behind the flotation tank (opposite to the camera) to illuminate microbubbles where the captured photos were processed using Dynamic Studio Software (Dantec Dynamics V5.1, Denmark). A threshold filter was applied to the images to facilitate the detection of micro-bubbles. The images were captured at 10°C, 20°C and 40°C for both fresh and saline water. To obtain the average size of the microbubbles, a minimum number of images was required which can be attained through convergence analysis. In convergence analysis, the mean bubble diameter and their standard deviation should reach a steady level as the number of detected targets increases. The mean bubble diameter ($\bar{d}$) and the standard deviation (σ) were calculated from Eqs. (8) and (9):

$$\bar{d} = \frac{1}{n}\sum_{i=1}^{n}\left(d_i\right) \tag{8}$$

$$\sigma = \left(\frac{1}{n-1}\sum_{i=1}^{n}\left(d_i - \bar{d}\right)^2\right)^{0.5} \tag{9}$$

where n and d_i are the number of bubbles and individual bubble diameter, respectively. To make sure that the calculated mean bubble diameter ($\bar{d}$) was close to the true mean (μ), a 95% of confidence interval ($\bar{d} - E < \mu < \bar{d} + E$) was estimated [23]. Here, E is the maximum difference between the observed sample mean ($\bar{d}$) and the true mean value (μ) defined as:

$$E = Z_{\alpha/2}\frac{\sigma}{\sqrt{n}} \tag{10}$$

where $Z_{\alpha/2}$ = 1.96 for a 95% confidence interval and n is the number of bubbles.

3. Results and discussion

In this section, firstly, effects of salinity and temperature on air solubility under equilibrium status are discussed. Secondly, the effects of both salinity and temperature were investigated for non-equilibrium conditions by considering saturator pressure and recycle ratio. Finally, the size distribution of microbubbles under influence of salinity and temperature were considered.

3.1. Equilibrium experiments

Fig. 3 represents the air concentration in recycled flow vs. aeration time for fresh water. As the figure shows, by increasing aeration time, the air concentration also increases up to a certain amount of concentration, where it reaches equilibrium status and doesn't change greatly. One noticeable finding in Fig. 3 is that as temperature increases, equilibrium time becomes shorter. For example, the equilibrium time is around 60 min at 40°C whereas it is around 250 min for 10°C. This significant difference in equilibrium time can be justified by the effect of temperature on the rate of the gas transfer into the body of the liquid phase. The rate of the gas/liquid mass transfer is controlled by a factor known as diffusivity factor which is defined as below [8]:

$$D = \frac{Tk'}{6\pi\alpha\mu} \tag{11}$$

where D is the diffusivity factor of the gas ($m^2\ s^{-1}$), k' is Boltzmann constant (1.38×10^{-23}), T is the absolute temperature (°K), α is the radius of the solute molecule (m), and μ is the viscosity of the solvent ($kg\ m^{-1}\ s^{-1}$). Increasing temperature reduces viscosity which results in the increase of diffusivity factor. On the other hand, gas transfer into the body of the liquid phase is controlled by the thickness of the gas–liquid interface, where the increase in temperature reduces the thickness of this boundary layer and facilitates the gas transfer by molecular diffusion. Accordingly, the equilibrium status can be achieved in shorter times for high temperatures [24].

The theoretical and experimental equilibrium concentrations are plotted in Fig. 4. As shown, both theoretical and experimental values follow a downward trend which is aligned with Henry's laws of gas dissolution in the liquid phase. In other words, the rise of the temperature increases Henry's constants, which consequently reduce air solubility [21]. A deeper look at Fig. 4 also shows that the calculated theoretical values are higher than the experimental values. Several factors such as reactor type and it geometry installed valves or pipes, and impurities in the water can contribute to this difference and lower the saturator efficiency. Additionally, both the theoretical and experimental values demonstrate that the addition of salt reduces the amount of dissolved air. Therefore, not only does temperature reduce air solubility, salinity decreases air solubility as well, which is consistent with Henry's laws of solubility under equilibrium conditions [21]. Haarhoff and Edzwald [6], in a theoretical study, assumed the equilibrium status for the air saturators

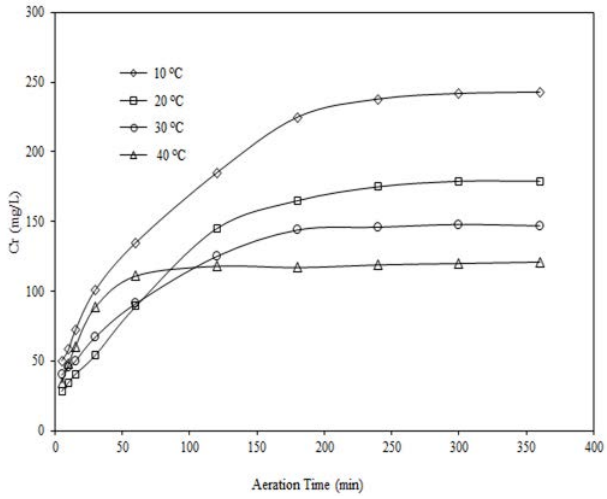

Fig. 3. Effect of aeration time on air solubility (pressure: 500 kPa, recycle ratio: 10%, air flow: 100 L h^{-1} and fresh water).

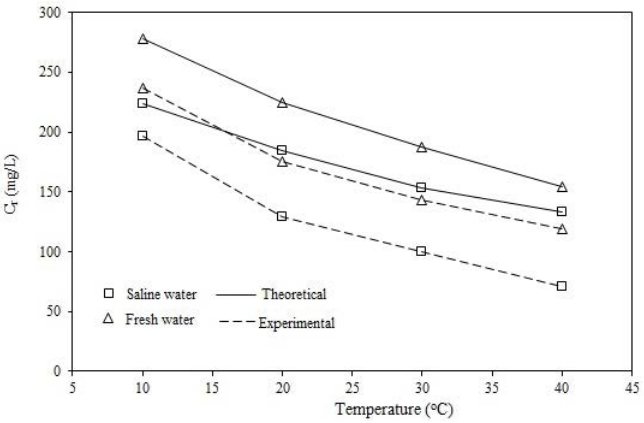

Fig. 4. Effect of temperature on theoretical and experimental air concentration for saline and fresh water (pressure: 500 kPa, recycle ratio: 10% and air flow: 100 L h^{-1}).

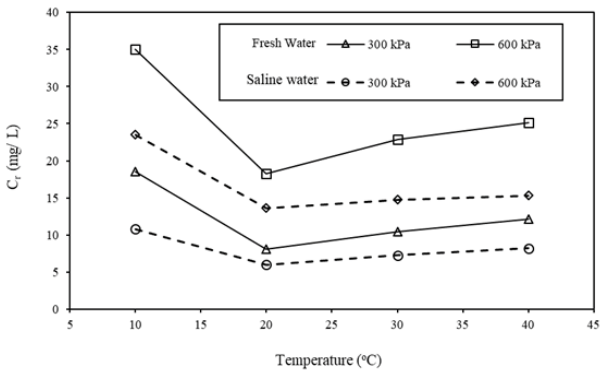

Fig. 5. Effect of temperature on dissolved air in recycled flow (air flow: 100 N h^{-1} and recycle ratio: 30%).

and showed that both salinity and temperature reduce air solubility.

3.2. Non-equilibrium experiments

The experimental results in Fig. 5 show that, regardless of salinity, the measured air concentration continuously decreases to a minimum value at 20°C and rises again with further increases in temperature. Correspondingly, the observed trend doesn't follow Henry's law of gas dissolution in the liquid phase as Henry's laws are defined for the equilibrium conditions. The HRTs for the range of the recycled flow (40 to 160 L h^{-1}) were calculated using Eq. (12) and listed in Table 2. As can be seen, the maximum HRT is 15 mins which implies that the system was operated in non-equilibrium conditions.

$$\mathrm{HRT} = \frac{Q_{\mathrm{Re}}}{V_{\mathrm{sat}}} \tag{12}$$

where Q_{Re} (L h^{-1}) is the amount of recycled flow and V_{sat} (L) is the volume of the air saturator cylinder.

The observed trend in Fig. 5 can be explained by the effect of temperature on gas/liquid mass transfer rate defined by Eq. 13 [24]:

$$\frac{dC}{dt} = K_L a\left(C_\infty - C_t\right) \tag{13}$$

where C_t (mg L^{-1}) is the concentration of the gas at time t, C_∞ (mg L^{-1}) is the equilibrium concentration, K_L (S^{-1}) is the mass transfer coefficient, and a (m^2) is specific interfacial area. The combination of $K_L a$ is known as the volumetric mass transfer coefficient. The mass transfer coefficient K_L can be affected by physicochemical properties of the gas and liquid phase such as viscosity, surface tension, diffusivity and density. Lee and Foster* [25] reviewed previous studies and found that the increase of temperature can affect these physicochemical parameters to some extent and finally increase the mass transfer coefficient (K_L). They also discovered that diffusivity factor is more influential compared to other parameters [25]. As mentioned before in Eq. (11), the increase of temperature increases diffusivity factor (D), which therefore increase mass transfer K_L coefficient. However, it also adds to the vapour content of bubbles and enlarges their size. This reduces the interfacial area and decreases the volumetric mass transfer coefficient ($K_L a$) after reaching a specified temperature. Additionally, growth of the bubbles increases the bubbles rising velocities which reduces their retention time and leads to less air dissolution [26]. Fig. 4 also shows that the rate of increase of available air after 20°C for saline water was less than fresh water. This can be explained by the effect of salinity on molecular diffusivity of the solute. In fact salinity decreases molecular diffusivity of the solute which in turn reduces the mass transfer coefficient [25,27]. Further, salinity increases viscosity which reduces the degree of turbulence and increases the boundary layer thickness reducing gas/liquid mass transfer. [28,29]. Until now, there have been only two studies in which the effects of temperature have been investigated, and both of these studies observed that firstly, equilibrium status was not obtained and secondly, air dissolution behaviour doesn't follow Henry's law of gas dissolution. Additionally, under non-equilibrium conditions, the amount of dissolved air was much lower compared to equilibrium status [8,19].

Table 2
Hydraulic retention times for different recycled flows for the influent flow of 400 L h^{-1}

Recycled flow (L h^{-1})	Recycle ratios (%)	Hydraulic retention time (min)
40	10	15
80	20	7.5
120	30	5
160	40	3.75

3.3. Effects of recycle ratio and saturator pressure

Fig. 6 indicates the effect of recycle ratio on air concentration in the recycled flow for different temperatures. As can be seen, regardless of temperature variations and

salinity, the air concentration reduces as recycle ratio increases. This can be attributed to the fact that HRT decreases as the recycle ratio increases. It is noteworthy to mention here that the measured air concentration in recycled flow (C_r) can be correlated to air concentration in the contact zone (C_b) in Eq. (14) [14]:

$$C_b = \left(\frac{r}{1+r}\right) \times C_r \tag{14}$$

where C_b (mg L^{-1}) is the air concentration in the flotation tank, C_r (mg L^{-1}) is the air concentration in the recycled flow and r is the recycle ratio.

With regard to Fig. 6, there is a negligible difference in air concentration beyond 20°C for each recycle ratio. Following the reason mentioned earlier, an increase in temperature above 20°C leads to an increase in air concentration. Accordingly, after 20°C, the increase of temperature is a contributive factor to air concentration, and there is no need to increase the recycle ratio to compensate for the shortage of air caused by temperature. However, below 20°C, there is a significant difference in the air concentration for different recycle ratios, and increasing the recycle ratio can compensate for the shortage of air caused by temperature. Additionally, regardless of temperature variations, increasing the recycle ratio can offset the lack of air concentration caused by salinity.

Fig. 7 shows the effect of pressure on the available air for different temperatures for both saline and fresh water. The results show that by increasing pressure, the air concentration (C_r) increases. However, there is a small difference in air concentrations for temperatures beyond 20°C at different saturator pressures for both saline and fresh water. This small difference is because temperature slightly increased the air concentration after 20°C. As shown above, since the air concentration is lower in saline water than fresh water for a fixed pressure, one approach to compensate for the lack of available air is to increase the operating pressure. For example, data in Fig. 7 show that if at 20°C, 10 mg L^{-1} of air is required in the recycled flow, the required pressure is 375 kPa, whereas, for the same air concentration and temperature, pressure should be increased to 500 kPa for the saline water. In addition to the effect of salinity, the effect of the temperature should also be considered. For example, if 10 mg L^{-1} of air is required in the recycle flow for saline water, this can be attained at 300 kPa pressure, whilst for the same amount of air at 20°C, the pressure should be increased to 500 kPa. For the above 20°C, as shown in Fig. 7, the lack of available air due temperature can be compensated by a slight increase of pressure, which is of great importance in terms of power consumption.

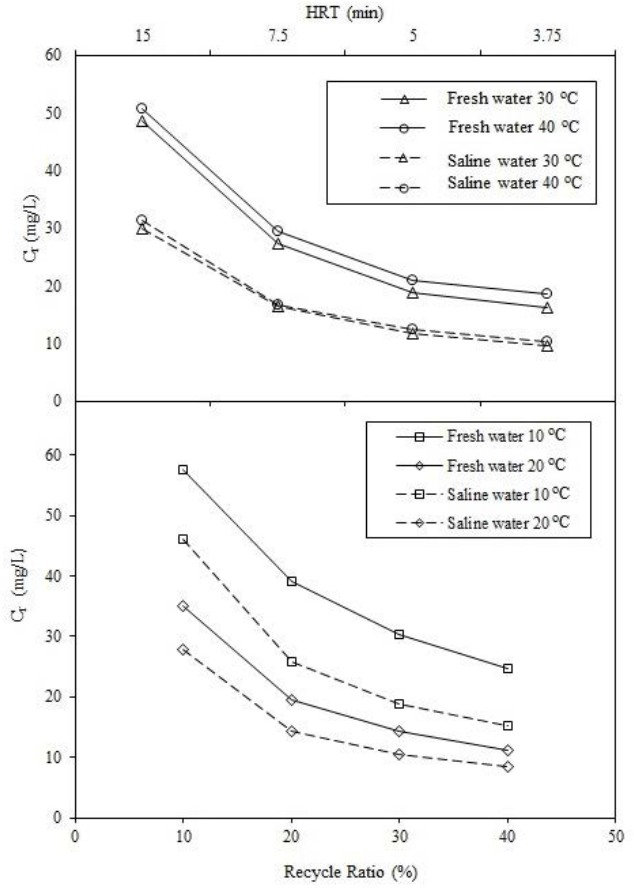

Fig. 6. Effect of recycle ratio on dissolved air in recycled flow (C_r), pressure: 500 kPa and air flow: 100 N h^{-1}.

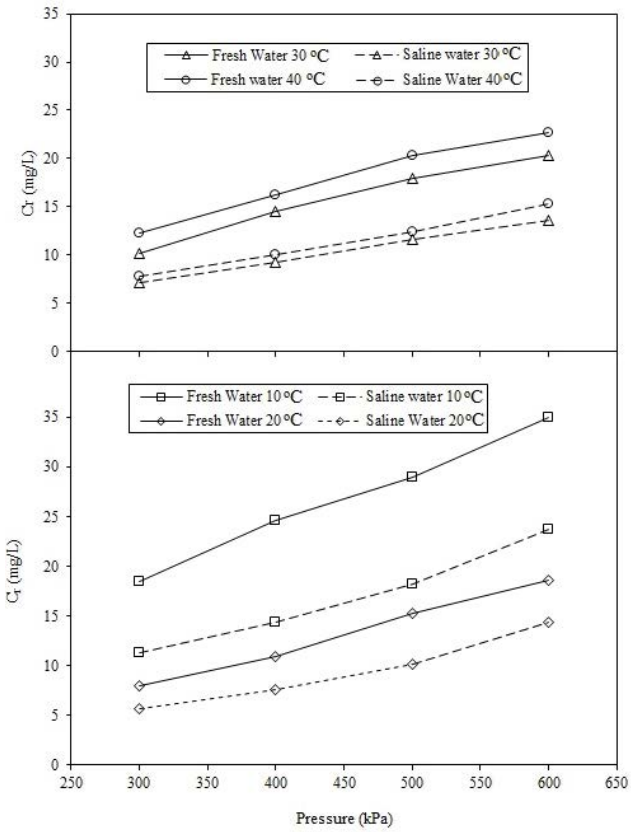

Fig. 7. Effect of pressure on dissolved air (recycle flow 30% and air flow: 100 L h^{-1}).

3.4. Bubble size distribution

Fig. 8 indicates the histograms of BSD in both saline and fresh water for different temperatures (10°C, 20°C and 40°C). The final mean diameter of microbubbles is also listed in Table 3. Fig. 8 shows that, by increasing temperature, the mean diameter of microbubbles decreases. This inverse relationship can be justified by Eq. (15) [30]:

$$d_{cd} = \frac{4\sigma}{\Delta P} \tag{15}$$

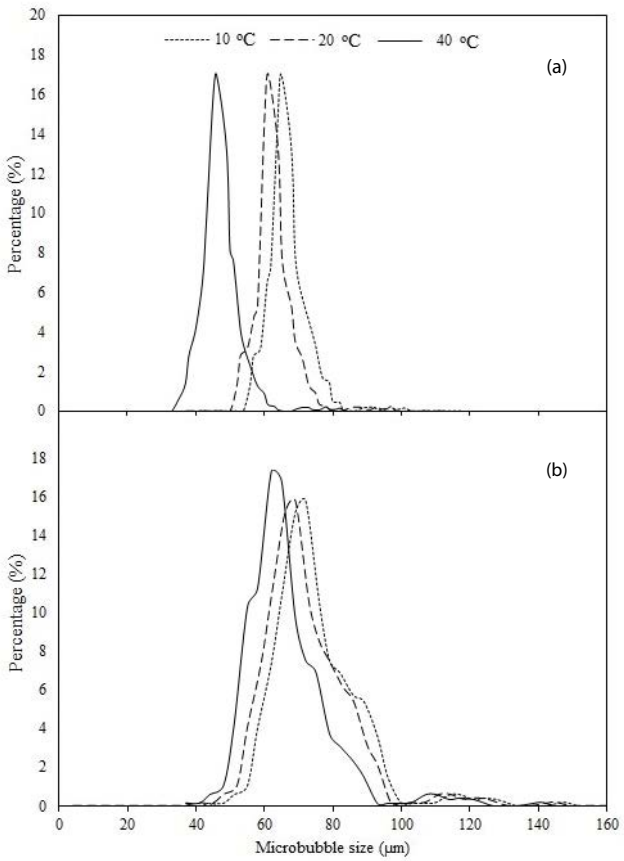

Fig. 8. Size distribution of microbubbles for saline water (a) and freshwater (b) (pressure: 500 kPa, recycled flow: 30% and airflow: 100 L h^{-1}).

where d_{cd} (m) is the critical size of microbubbles, σ (N/m) is the surface tension of the water, and ΔP (N/m^2) is the pressure difference across the injection device. Eq. (15) can explain the changes of the size due to the temperature as there is an inverse relation between surface tension (σ) and temperature. In other words, by increasing temperature, surface tension decreases which results in smaller size microbubbles. On the other hand, Fig. 8 indicates that the size of microbubbles is inversely proportional to the salinity which is not consistent with Eq. (15) as salinity increases surface tension [22]. The reduction in the size is related to the repulsive hydration force which prevents the coalescence of two adjacent microbubbles. This force is caused by the formation of the water molecules close to charged surfaces, and can be calculated by Eq. (16) [31]:

$$\Pi_{hyd} = \left(\frac{W}{\lambda}\right)\exp\left(\frac{-h}{\lambda}\right) \tag{16}$$

where W is the pre-exponential constant (≈6 m N/m^2), λ is the decay length of the hydration interaction mostly taken the value of 8.5 nm, and h is the film rapture thickness. Cain and Lee [31] measured the film rapture thickness (h) and found that as salinity increases, film rupture thickness decreases. With regards to Eq. (14), salinity increases repulsive hydration force and delays the coalescence of bubbles.

There are also some other inhibitive forces which prevent the coalescence of bubbles such as Van der Waals force and dielectric double layer force. Nevertheless, the values of these forces are negligible and can be disregarded [31]. In a few studies, salinity has been identified as an inhibitive parameter suppressing the coalescence [32–34]. Kawahara et al. [35] also measured the size distribution of microbubbles in saline and tap water in a flotation column. They found that salinity decrease the size of bubbles by suppression of coalescence.

4. Conclusions

The present study investigates the effects of salinity and temperature on air dissolution in an unpacked air saturator. It was observed that under equilibrium conditions, air dissolution follows Henry's law of gas dissolution in the liquid phase and air solubility steadily decreases as temperature and salinity increase. However, in real scale applications, equilibrium status is seldom achieved as it demands a huge amount of retention time. Even though

Table 3
Convergence analysis for fresh and saline water

Type of water	Temperature (°C)	Convergence number of bubbles	Final mean diameter (μm)	Final standard deviation (μm)	Final confidence of interval (μm)	Minimum required images (n_{re})
Fresh water	10	4,000	75	54	7.2	659
	20	7,500	74	55	8.3	1,236
	40	5,500	63	68	8.7	907
Saline water	10	5,200	73	43	8.4	906
	20	8,600	68	50.5	8.5	1,416
	40	6,300	58	46	8.5	1,037

the amount of dissolved air under equilibrium condition is much higher than the non-equilibrium status, the operation of DAF systems under a non-equilibrium status can acquire the required air concentration for the removal of suspended particles in low turbidity effluents (up to 10 NTU). This can significantly reduce the associated costs with the size of air saturator and the operation of the DAF systems. Accordingly, air dissolution behaviour has also been studied under normal operation of the DAF system, and it was observed that, under non-equilibrium status, air dissolution is controlled by the type of the reactor, liquid properties, and operating conditions which affect volumetric gas/liquid mass transfer (K_La). Therefore, operators should consider abovementioned parameters for each air saturator in order to reduce costs and a more efficient DAF system.

In the design of a DAF system, the required amount of air in the flotation tank is determined by the available suspended solids. Therefore, it is rational to have the same amount of air for both saline and fresh water. To compensate for the lack of the available air caused by salinity and temperature, increases of recycle ratio and saturator pressure are two alternative solutions. As for the air saturator in this study:

- Regardless of temperature variations, the lack of air concentration caused by salinity can be compensated by increasing recycle ratio and saturator pressure.
- For temperatures below 20°C, increases of recycle ratio or saturator pressure help to elevate the lack of air concentration caused by increase of temperature.
- For temperatures above 20°C, an increase of temperature by itself contributes to the increase of air concentration, where there is no need to increase the recycle ratio or operating pressure. This is of great importance in terms of energy consumption and costs.

Finally, changes in temperature don't affect the size distribution of microbubbles remarkably, however, the existence of salt can prevent coalescence and results in smaller size microbubbles.

Acknowledgment

The authors would like to thank Mr. Abdellah Shafieian for his valuable comments on the experimental procedures of this study.

References

[1] J.K. Edzwald, Dissolved air flotation and me, Water Res., 44 (2010) 2077–2106.
[2] J.K. Edzwald, Principles and applications of dissolved air flotation, Water Sci. Technol., 31 (1995) 1–23.
[3] A. Besson, P. Guiraud, Characterization of Bubbles Produced by Dissolved Air Flotation in Saline Water, in Flotation for Water and Wastewater Systems, IWA, New York, USA, 2012.
[4] S.E. Burns, S. Yiacoumi, C. Tsouris, Microbubble generation for environmental and industrial separations, Sep. Purif. Technol., 11 (1997) 221–232.
[5] S.-H. Kim, C.-S. Min, S.K. Lee, Application of dissolved air flotation as pretreatment of seawater desalination, Desal. Wat. Treat., 33 (2011) 261–266.
[6] J. Haarhoff, J.K. Edzwald, Adapting dissolved air flotation for the clarification of seawater, Desalination, 311 (2013) 90–94.
[7] T. Kim, T. Temesgen, H. Park, M.Y. Han, Physical characteristics of bubbles in dissolved air flotation processes in seawater reverse osmosis desalination plants, Desal. Wat. Treat., 70 (2017) 19–23.
[8] A. Dassey, C. Theegala, Optimizing the air dissolution parameters in an unpacked dissolved air flotation system, Water, 4 (2011) 1–11.
[9] S. Steinbach, J. Haarhoff, Air transfer efficiency of packed saturators used in DAF, J. AWWA, 89 (1997) 71–82.
[10] V.R. Fanaie, M. Khiadani, T. Ayres, Effects of internal geometry on hydrodynamics of dissolved air flotation (DAF) tank: an experimental study using particle image velocimetry (PIV), Colloids Surf., A, 575 (2019) 382–390.
[11] D.M. Leppinen, S.B. Dalziel, Bubble size distribution in dissolved air flotation tanks, J. Water Supply Res. Technol. AQUA, 53 (2004) 531–543.
[12] J. Edzwald, J. Haarhoff, Dissolved Air Flotation for Water Clarification, McGraw Hill Professional, U.S.A., 2011.
[13] J. Haarhoff, S. Steinbach, A comprehensive method for measuring the air transfer efficiency of pressure saturators, Water Res., 31 (1997) 981–990.
[14] A. Bahadori, G. Zahedi, S. Zendehboudi, M. Bahadori, Estimation of air concentration in dissolved air flotation (DAF) systems using a simple predictive tool, Chem. Eng. Res. Des., 91 (2013) 184–190.
[15] R.A. Conway, R.F. Nelson, High Solubility Gas Flotation in Liquid–Solid Separation, Google Patents, 1981.
[16] D.A. Lovett, S.M. Travers, R.L. Maas, Treatment of abattoir wastewater by dissolved air flotation. Part 1. - wastewater not pretreated, Meat Res. Report, 9 (1984) 1–35.
[17] J.G. Henry, R. Gehr, Dissolved air flotation for primary and secondary clarification, Sewage Collection and Treatment Report SCAT-9, Project sponsored by Canada Mortgage & Housing Corporation and Environment, Canada, 1981.
[18] S. Steinbach, J. Haarhoff, A simplified method for assessing the saturation efficiency at full-scale dissolved air flotation plants, Water Sci. Technol., 38 (1998) 303–310.
[19] W.T. Shannon, D.H. Buisson, Dissolved air flotation in hot water, Water Res., 14 (1980) 759–765.
[20] J. Haarhoff, S. Steinbach, A model for the prediction of the air composition in pressure saturators, Water Res., 30 (1996) 3074–3082.
[21] R. Sander, Compilation of Henry's law constants (version 4.0) for water as solvent, Atmos. Chem. Phys., 15 (2015) 4399–4981.
[22] K.G. Nayar, M.H. Sharqawy, L.D. Banchik, Thermophysical properties of seawater: a review and new correlations that include pressure dependence, Desalination, 390 (2016) 1–24.
[23] R.E. Walpole, R.H. Myers, S.L. Myers, K. Ye, Probability and statistics for engineers and scientists, Vol. 5,Macmillan, New York, 1993.
[24] K. Akita, F. Yoshida, Bubble size, interfacial area, and liquid-phase mass transfer coefficient in bubble columns, J. Ind. Eng. Chem., 13 (1974) 84–91.
[25] J.H. Lee, N.R. Foster*, Measurement of gas-liquid mass transfer in multi-phase reactors, Appl. Catal., 63 (1990) 1–36.
[26] Y. Zhu, J. Wu, Gas/liquid mass transfer in hot sparged systems, Dev. Chem. Eng. Min. Process, 12 (2004) 323–332.
[27] A. Suresh, T. Sridhar, O. Potter, Mass transfer and solubility in autocatalytic oxidation of cyclohexane, AIChE J., 34 (1988) 55–68.
[28] C. Chapman, L. Gibilaro, A. Nienow, A dynamic response technique for the estimation of gas—liquid mass transfer coefficients in a stirred vessel, Chem. Eng. Sci., 37 (1982) 891–896.
[29] H. Yagi, F. Yoshida, Gas absorption by Newtonian and non-Newtonian fluids in sparged agitated vessels, Ind. Eng. Chem. Process Des. Dev., 14 (1975) 488–493.
[30] A.A. Kulkarni, J.B. Joshi, Bubble formation and bubble rise velocity in gas–liquid systems: a review, Ind. Eng. Chem. Res., 44 (2005) 5873–5931.
[31] F.W. Cain, J.C. Lee, A technique for studying the drainage and rupture of unstable liquid films formed between two captive bubbles: measurements on KCl solutions, J. Colloid Interface Sci., 106 (1985) 70–85.
[32] V.S.J. Craig, B.W. Ninham, R.M. Pashley, Effect of electrolytes on bubble coalescence, Nature, 364 (1993) 10192–10197.

[33] L.A. Del Castillo, S. Ohnishi, R.G. Horn, Inhibition of bubble coalescence: Effects of salt concentration and speed of approach, J. Colloid Interface Sci., 356 (2011) 316–324.
[34] D.K. Ruen-ngam, P. Wongsuchoto, A. Limpanuphap, T. Charinpanitkul, P. Pavasant, Influence of salinity on bubble size distribution and gas–liquid mass transfer in airlift contactors, Chem. Eng. J., 141 (2008) 222–232.
[35] A. Kawahara, M. Sadatomi, F. Matsuyama, H. Matsuura, M. Tominaga, M. Noguchi, Prediction of micro-bubble dissolution characteristics in water and seawater, Exp. Therm Fluid Sci., 33 (2009) 883–894.
[36] R.J. Moffat, Using uncertainty analysis in the planning of an experiment, J. Fluids Eng., 107 (1985) 173–178.
[37] J.P. Holman, Experimental Methods for Engineers, 8th ed., McGraw-Hill, U.S.A., 2011.

Appendix

A1. Experimental uncertainties

The range of the parameters in this study with their intervals and uncertainties are listed in Table1. The total uncertainty was calculated from standard deviation method defined as [36]:

$$W_t = \sqrt{\varepsilon_s^2 + \varepsilon_r^2} \tag{A1}$$

where, W_t is the total uncertainty ε_s and ε_r are systematic and random errors, respectively, and defined as:

$$\varepsilon_s = \sqrt{\sum_{i=1}^{n} \varepsilon_{s,i}^2} \tag{A2}$$

$$\varepsilon_r = \sqrt{\sum_{i=1}^{n} \varepsilon_{r,i}^2} \tag{A3}$$

In these equations, n is the error source number and $\varepsilon_{r,i}$ is calculated from:

$$\varepsilon_{r,i} = \sqrt{\frac{\sum_{i=1}^{n} \left(\varphi_i - \bar{\varphi}\right)^2}{N\left(N-1\right)}} \tag{A4}$$

where N and $\bar{\varphi}$ are the number of repetitions of a parameter and the average value, respectively.

The propagation of errors method was used to estimate the uncertainty of the calculated quantities. According to Holman [37], the uncertainty of the results (W_R) can be calculated from:

$$W_R = \sqrt{\sum_{i=1}^{n} \left(\frac{\partial R}{\partial x_i} W_i\right)^2} \tag{A5}$$

where $R = R(x_1, x_2, \ldots, x_n)$, x represents an independent variable and W is the uncertainty in that variable.